THE JOURNAL OF PHYSICAL CHEMISTRY B

Article

pubs.acs.org/JPCB

Stability and Function at High Temperature. What Makes a Thermophilic GTPase Different from Its Mesophilic Homologue

Marina Katava,[†] Maria Kalimeri,[‡] Guillaume Stirnemann,[†] and Fabio Sterpone*[,†]

[†]CNRS (UPR9080), Institut de Biologie Physico-Chimique, Université de Paris Sorbonne Cité et Paris Science et Lettres, Univ. Paris Diderot, Laboratoire de Biochimie Théorique, 13 rue Pierre et Marie Curie, 75005, Paris, France

[‡]Department of Physics, Tampere University of Technology, Tampere, Finland

Supporting Information

ABSTRACT: Comparing homologous enzymes adapted to different thermal environments aids to shed light on their delicate stability/function trade-off. Protein mechanical rigidity was postulated to secure stability and high-temperature functionality of thermophilic proteins. In this work, we challenge the corresponding-state principle for a pair of homologous GTPase domains by performing extensive molecular dynamics simulations, applying conformational and kinetic clustering, as well as exploiting an enhanced sampling technique (REST2). While it was formerly shown that enhanced protein flexibility and high temperature stability can coexist in the apo hyperthermophilic variant, here we focus on the holo states of both homologues by mimicking the enzymatic turnover. We clearly show that the presence of the ligands affects the conformational landscape visited by the proteins, and that the corresponding state principle applies for some functional modes. Namely, in the hyperthermophilic species, the flexibility of the effector region ensuring long-range communication and of the P-loop modulating ligand binding are recovered only at high temperature.

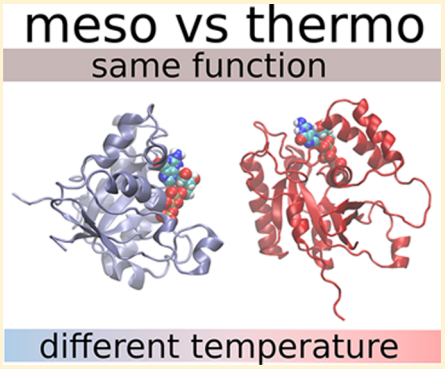

INTRODUCTION

Thermophilic organisms thrive in hot environments that challenge the stability of their molecular constituents.[1] In particular, thermophilic enzymes are not only stable at high temperatures—in some cases as high as the boiling point of water (100 °C)—but generally function optimally in this extreme regime only. In fact, they show little, if any, activity at ambient conditions.[2]

A corresponding state scenario[3,4] was proposed in order to rationalize the stability/function trade-off of thermophilic enzymes when compared to their mesophilic homologues. According to the principle, the shift of thermal stability and activity in thermophiles is due to enhanced mechanical rigidity of the protein matrix. The mechanical rigidity is viewed as emerging from the enthalpic stabilization of the protein fold that arises from specialized intramolecular interactions like ion pairs, hydrophobic contacts, and hydrogen bonds.[1,5−8] The lack of activity at ambient conditions is due to the quenching of some functional modes that are conversely activated at high temperatures.[2,9]

The universality of the rigidity paradigm was investigated and questioned along the years both experimentally[10−12] and theoretically.[13−18] Early hydrogen/deuterium (H/D) experiments probing the exposure of amide groups to solvent by local unfolding revealed agreement between the protective factors of mesophilic and thermophilic proteins at their respective optimal working temperatures.[5,10,19] Notwithstanding, using the same technique, high local flexibility, comparable to what is found in mesophilic proteins, was measured at ambient conditions for the very thermostable enzyme rubredoxin from *Pyrococcus furiosus*.[11] An attempt to establish a direct link between protein activity and local flexibility was pursued by complementing kinetic experiments monitoring the enzymatic turnover and H/D measurements on a pair of homologous alcohol dehydrogenases (ADHs).[12,20] The corresponding state scenario was reported for the hydrogen tunnelling contribution to the chemical step of the enzymatic reaction, where the thermophilic ADH from *Bacillus stearothermophilus* showed an important contribution from the tunnelling at high temperature only (65 °C), while the mesophilic ADH exhibited a similar contribution at ambient conditions (25 °C). However, the rationale behind the thermal activation of the tunnelling in the thermophilic enzyme still remains elusive.[12,20,21] Intense focus has also been placed on homologous dihydrofolate reductases,[22−24] where additional complexity in comparing temperature dependent activities is introduced owing to the fact that the mesophilic enzyme is monomeric, while the active form of the thermophilic variant is dimeric. The dimeric state is suggested to filter accessible conformations by constraining the catalytically important loops at the dimer interface. This is thought to prevent the electrostatic preorganization of the

Received: January 11, 2016
Revised: February 23, 2016
Published: February 23, 2016

DOI: 10.1021/acs.jpcb.6b00306
J. Phys. Chem. B 2016, 120, 2721−2730

active site[21] and the consequent lowering of the kinetic barrier for the enzymatic reaction.[14,24]

Similarly, the propagation of domain interfacial constraints on the nanosecond time scale, probably modulated by the presence of internal water,[25] was observed in simulations of a pair of malate dehydrogenases[26] in the loop that gates substrate binding, with the thermophilic variant characterized by an occluded binding site at ambient conditions. However, the simulations at high temperature could not probe the thermal activation of the corresponding mode. NMR relaxation experiments singled out the relative domain motion that controls the open/closed kinetics of the catalytic site, and its thermal response, as the principal mode differentiating mesophilic and thermophilic adenylate kinases.[27] When focusing on fast modes, i.e. the atomistic fluctuations probed by small angle neutron scattering (NS), the corresponding state principle was not verified for two malate dehydrogenases; in fact, the thermophilic homologue manifests larger atomistic displacements than the mesophilic variant that are also less sensitive to temperature;[28] however, again, the microscopic interpretation of the experimental signal was later questioned.[29] On the contrary, a combined NS and molecular modeling study reported the validity of the corresponding state hypothesis for the thermobarophilic protein IF-6 subject to both thermal and pressure stress.[30]

Despite extensive research, the direct connection between the thermal activation of protein flexibility and the temperature dependence of the enzymatic activity remains elusive. In fact, it is plausible that mechanical rigidity controls the stability of the protein by ensuring a functional fold at high temperature, while the temperature shift of the activity depends solely on a higher kinetic barrier for the enzymatic chemical step.[14,21] However, when allostery or conformational changes control substrate binding and unbinding or signal propagation upon catalysis, thermal activation of relevant modes has to be considered in detail.

In this work, we tackle the problem by considering a model system, a pair of homologous G-domains from a mesophilic (Elongation-Factor Tu) and a hyperthermophilic (Elongation-Factor 1α) protein. The Elongation-Factor (EF)[31,32] participates in protein translation, which takes place in the ribosome. The EF carries an aminoacyl-tRNA (aa-tRNA) to the ribosome, where the mRNA is translated to an amino-acid sequence by pairing its nucleotide bases with those of the aa-tRNA. Initially, the EF forms a ternary complex EF·GTP·aa-tRNA, and upon codon-anti codon recognition, the GTP is hydrolyzed to GDP, inducing a conformational change necessary for the release of the aa-tRNA and dissociation from the ribosome in the EF·GDP form. The interested readers can find a substantial body of work where the catalytic boost of the GTPase activity[33] as well as the EF conformational changes[34−37] induced by ribosome binding were deeply investigated.

The EF-Tu of *E. coli* and EF-1α of *S. solfataricus* are of similar structure,[38−41] both triangular three-domain proteins with a hole in the middle and substantial differences between the reactant GTP (active) and product GDP (inactive) state. Despite the role of interdomain interactions ensuring long-range communication, some essential features of the EF activity can be investigated by considering only the catalytic domain, as the isolated domain is catalytically active.[42,43] The catalytic subunit is slightly less thermostable than the three-domain protein for both the mesophile and the thermophile. The inactivation temperature of the catalytic subunit in the EF-Tu is 41 °C as opposed to 46 °C for the entire protein;[44,45] for EF-1α, the catalytic subunit loses activity at 84 °C and the entire protein at 94 °C.[43] These temperatures are close to the optimum growth temperatures of *E. coli* (37 °C) and *S. solfataricus* (80 °C), confirming that the proteins are optimized to function in a narrow temperature window.

Moreover, the important conformational changes during the enzymatic turnover[46,47] occur in some specific regions of this domain. In the mesophilic domain, the crystallographic structures of the reactant and the product states show marked differences in the switch I region (also referred to as effector region, residues G40−I62) and switch II region (G83−T93). The former is reported to undergo a dramatic α to β secondary structure transition between residues P53 and G59 upon GTP hydrolysis,[48,49] while the latter is a helix that shifts towards the C-terminus by a single turn.[38] The structure also contains a number of conserved residues, most notably in the P-loop (G18−T25) and in the region between residues N135 and D138, both lining the active site and forming hydrogen bonds with the ligand.

The switch I region of the hyperthermophilic variant contains an insertion of two small α helices, and no conformational change spanning this region was reported in the literature. Computer simulations[16] showed that the early steps of the protein unfolding in the mesophilic G-domain occur at the level of the switch I region, indicating that the structuring effect due to the helical insertions is an essential stabilizing factor for the hyperthermophilic species.

In order to get more precise insight on the rigidity/function relationship, we used computer simulations to investigate the two homologous G-domains in their holo states by virtually mimicking the enzymatic turnover. Molecular dynamics of the protein−substrate complexes were performed at the microsecond time scales. Enhanced sampling of the protein conformations was also performed by employing the Hamiltonian-replica exchange scheme REST2.[50,51]

Here we verify the validity of the corresponding state principle for some key functional modes of the proteins in their holo state. Namely, we show that the magnitude of the changes in the flexibility upon GTP binding and hydrolysis are comparable between the two species at their respective "optimal working" temperatures. Moreover, we confirm that the stability/function trade-off is encoded in the structural motif of the switch I region, which is highly flexible and keen to secondary structure shift in the mesophilic species, while being highly structured and more resistant to temperature in the hyperthermophilic domain.

METHODS

Systems. We have studied the isolated catalytic G-domain of the mesophilic (*E. coli*) EF-Tu and that of the hyperthermophilic (*S. solfataricus*) EF-1α. The mesophile domain was considered in the apo state and with the GTP or GDP molecules bound to its active site. Depending on the nature of the ligand bound to the protein, the switch I region (P53−G59) is α-helical in the crystal structure isolated in the presence of GTP (PDB 1OB2), while it is a β-sheet when GDP is present (1EFC).[38] Both conformers have been considered, leading to a total of six systems for the mesophilic domain: the two apo conformers, ecG$^{\alpha}$ and ecG$^{\beta}$, and the two holo states in all of their possible conformations, leading to four additional states ecG$^{\alpha}$·GTP, ecG$^{\alpha}$·GDP, ecG$^{\beta}$·GTP, and ecG$^{\beta}$·GDP. The catalytic G-domain of the hyperthermophilic EF-1α was

DOI: 10.1021/acs.jpcb.6b00306
J. Phys. Chem. B 2016, 120, 2721−2730

extracted from the PDB entry 1SKQ,[40] with the missing portion spanning the residues 66 to 76 inserted by homologous modeling.[52] In the crystal structure, the protein was isolated with GDP bound to it, which was either removed, kept intact, or replaced by GTP to simulate the apo, holo ssG·GDP, and ssG·GTP states, respectively.

Molecular Dynamics Simulations. The G-domains were capped with COO^- and NH_3^+ terminals. Ligands, when not originally present in the crystallographic structures, as in the case of GTP, were aligned to an existing substrate (GDP or GNP). A short minimization was performed to relax structural clashes. The proteins were inserted in a simulation box and solvated with water by surrounding the protein with at least a 10 Å layer of solvent. Ions were added to neutralize the systems. All the simulations have been carried out using the NAMD 2.9 software,[53] the CHARMM22/CMAP force field for the protein,[54,55] and the CHARMM-TIP3P model for water. After a 4-ns thermal equilibration, the simulations were propagated in the NPT ensemble using a Langevin thermostat (characteristic time 1 ps) and barostat (dumping time 50 fs). In the simulations, we used an integration time step of 2 fs. All systems were simulated at ambient conditions, T = 300 K and P = 1 atm, for 0.6 μs. The hyperthermophilic system was also simulated at a higher temperature, T = 380 K, mimicking the working condition of the enzyme. The short-range interactions and the real space contribution of electrostatic interactions were cut off at 12 Å, while the long-range contributions of electrostatic interactions were handled by the PME algorithm[56] with a grid spacing of 1 Å. All bonds involving hydrogens were constrained. The trajectories were recorded with a frequency of 4 ps.

REST2 (Replica Exchange with Solute Scaling). In order to enhance the conformational sampling of the switch I region, we used a recent implementation of REST2,[50,51] a Hamiltonian-exchange parallel tempering technique. The REST2 algorithm is based on the rescaling of some terms of the potential energy of the system, namely, the dihedral potential energy terms of the protein and the nonbonded protein−protein and protein−solvent interactions. This scaling may concern the protein in its entirety or a portion of it. Here we have thermally excited the switch I region of the two systems in the holo state. We used 12 replicas for the mesophilic systems and 16 for the hyperthermophilic ones, as the thermophilic system contains both a larger protein and a larger number of water molecules, thus needing a larger number of replicas to achieve similar replica exchange efficiency (40%). The replicas were allowed to exchange every 10 ps. According to a mean-field rescaling scheme,[51] the replicas scanned an effective temperature window of $T_{\mathrm{eff}} \in [280\ \mathrm{K}, 575\ \mathrm{K}]$ for the fragment. The rest of the system was thermalized at a reference temperature of 300 K. In order to avoid the finite-size effect on the sampling of the conformation of the switch I region, the proteins were solvated in a larger box with respect to those used in the MD setup. A total of about 14 000 and 18, 000 water molecules were used to solvate the mesophilic and hyperthermophilic proteins, respectively. The simulation protocol was similar to what was described for the standard MD simulations. In addition, for the mesophilic protein, REST2 simulations were also carried out using the CHARMM36 force field, in an attempt to sample the secondary structure of the switch I domain more faithfully.[57]

Conformational Clustering. The main analysis of the protein flexibility was based on conformational clustering that allows determining the number of representative conformational states visited by the system and the frequency of transitions between them. Networks of conformational states were built by using the root mean squared distance as a collective variable

$$\mathrm{RMSD}(t) = \sqrt{\frac{1}{N_{C_\alpha}} \sum_{i=1}^{N_{C_\alpha}} (r_i(t) - r_i^{\mathrm{reference}})^2} \quad (1)$$

where N_{C_α} is the number of carbon C_α atoms, and the "reference" structures are cluster leaders. The cutoff used for separating the states was 2.5 Å. Clustering was performed using the leader−follower algorithm.[58] For computational reason the trajectories were analyzed with a frequency of 20 ps. The details of the clustering procedure are given in ref 16. To test the robustness of our results, we also performed clustering using other collective variables, such as the fraction of native contacts and the fraction of native torsion angles,[16] all agreeing well in the observations presented in the discussion (see Tables S2 and S3 in the Supporting Information). The results of the clustering were visualized as a network of states by using a force based algorithm as implemented in GEPHI.[59]

Markov Clustering Algorithm. Conformational networks were further clustered using a Markov clustering algorithm.[60] This procedure allows one to separate kinetically relevant states. Random walks are generated starting from leader states obtained by the conformational clustering, and by using the frequency of their interconversion, a transition state matrix is built up. Two matrix operations, namely, expansion (i.e., matrix squaring) and inflation (i.e., taking the Hadamard power), are iteratively applied on the transition matrix until convergence is reached and the walkers are confined inside local minima by kinetic barriers. The method depends on a granularity parameter that sets the height of the kinetic barriers. The details of the implementation can be found in refs 16 and 60. Again, the kinetically grained clusters were represented as networks of interconverting states.

RESULTS AND DISCUSSION

Substrate Effects on Protein Conformations: the Mesophilic G-Domain. In this first section, we analyze the conformational changes induced by a ligand bound to the mesophilic ecG. The results are based on long MD simulations extending to the microsecond time scale (0.6 μs). Namely, by following the hypothetical enzymatic turnover of the protein, we have inquired into the equilibrium shift of protein conformational substates due to binding of the reactant (GTP) and product (GDP) molecules. The sequence of conformations accessed by the ecG during the EF-Tu activity are schematically represented in the bottom panel of Figure 1, according to the resolved X-ray structures.

We have performed conformational and kinetic clustering of the long MD trajectories (see Methods). The network representation of the complex conformational landscape was reconstructed highlighting both the population of the states and the frequencies of their interconversions; see Figure 2. We first discuss the results obtained for the "reactant" conformer ecG^{α}. Most notably, the protein gets stiffer when GTP binds to ecG^{α}. In fact, the number of conformational states accessed by the protein drops down by a factor of 5 as compared to the apo state; see also Table S1 in the Supporting Information. The region mainly affected by the GTP ligand is the switch I, which

DOI: 10.1021/acs.jpcb.6b00306
J. Phys. Chem. B 2016, 120, 2721−2730

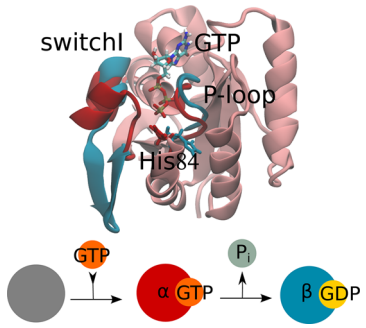

Figure 1. Top panel: the superimposition of the G-domain of *E. coli* EF-Tu in the active GTP form, where the switch I region (G40-I62) is in α secondary structure (shown in red), and the inactive GDP form, where the region is partially in the β state (shown in blue). The same color code is used to emphasize other important structural elements, the P-loop (G18-T25) lining the active pocket and the explicitly shown His84, discussed later in the text. GTP is shown in the active site. Lower panel: the catalytic cycle of the EF-Tu, and the corresponding conformational changes.

is highlighted in the bottom panel of Figure 2, where we have magnified the portions of the protein matrix exhibiting larger flexibility, measured by the atomistic mean squared fluctuations (msf) of C_α. When the GDP is bound to the same initial ecG$^\alpha$ structure, the sampled conformational landscape is less confined, and the protein preserves its intrinsic flexibility. A very similar behavior was recovered when, as the initial state, we considered an equilibrated configuration from the ecG$^\alpha$·GTP simulation and replaced GTP with GDP (simulation denoted ecG$^\alpha$·GDP(*)). Again, when the GDP molecule is bound to the domain, the flexibility of the protein is much higher than in the case of the GTP bound state (data shown in Table S1 of the Supporting Information). Apart from the switch I region, the flexibility of the protein is mostly concentrated in the switch II region, similar to what was previously observed in a MD simulation of the entire protein in the apo and holo GDP states.[61] It is important to note that the shift of protein stiffness upon ligand binding is also visible when considering the kinetic clustering of the trajectories on the basis of a Markov state model; see the Methods section. This type of clustering helps to visualize protein substates separated by high kinetic barriers (Figure 2). The contribution of the backbone flexibility to the entropy changes in the catalytic cycle has been calculated estimating the S^2 order parameter of the NH bond reorientation.[62,63] Data for the mesophilic and thermophilic species are reported in Table S4 in the Supporting Information, and add extra weight to the results obtained by conformational clustering, where the change in the number of cluster leaders implies a change in the probability of microstate occupancy, which is proportional to the overall entropy.

For the EF-Tu, a conversion from the α to β conformers follows the GTP hydrolysis according to the literature.[38,48] Therefore, it is convenient to examine the reshaping of the conformational landscape of the "product" conformer ecG$^\beta$. In this case, for both ligands, the general effect of substrate binding on the global protein flexibility is very weak. In fact, no dramatic changes are observed in the conformational and kinetic clustering of the generated trajectories.

While the exact sequence of conformational interconversions is not known and our data do not provide clues on the selective pathway along the enzymatic turnover, the conformational and kinetic clustering of the independent states suggests that heterogeneous kinetics for GTP hydrolysis could emerge as the effect of the conformational transitions.[64] These transitions would potentially filter substrate binding/unbinding as well as modulate the kinetic barrier of the chemical step. Understanding whether the transitions are specific to the mesophilic homologue or are shared with the more thermally stable ssG will help in clarifying the molecular mechanism of the thermal activation of the hyperthermophilic homologue. This will be addressed in the next sections.

In Quest of the Conformational Transition in the Mesophilic G-Domain. We have mentioned that the transition from the α toward the β conformer is expected to occur upon GTP → GDP conversion. This conformational change is a biologically relevant signal, as it triggers dissociation from the ribosome. Trapping the GDP state in the α configuration prevents this dissociation and thus stops the peptide translation, a fact exploited by some antibiotics.[65] The switch I region should therefore access the β state in the ecG$^\alpha$·GDP simulation, and similarly, transition toward the helical state is expected in the same region when GTP replaces GDP, i.e. in the ecG$^\beta$·GTP simulation. It should be mentioned that because of the small extension of the fragment of interest (P53−G59) it is difficult to observe extended β-strands. Even in the crystallographic structure, only two cross H-bonds are detected as β linkers. For this reason, hereby our definition of

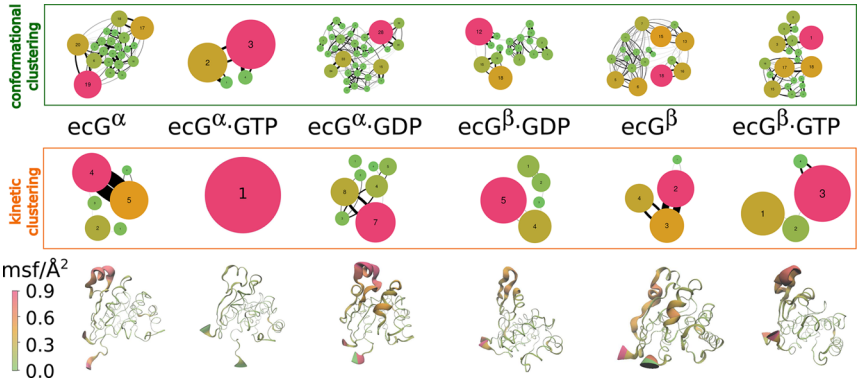

Figure 2. Conformational clusters shown in network representations for the protein with and without its ligands, with each node representing conformations with RMSD that differ by 2.5 Å. Nodes of kinetic networks show substates that are separated by high energy barriers, while a single node contains states separated by low energy barriers. The lowest panel represents the mean squared fluctuation, a measure of protein flexibility, shown in color and thickness of the protein backbone. Data refer to the MD simulations performed at T = 300 K.

DOI: 10.1021/acs.jpcb.6b00306
J. Phys. Chem. B 2016, 120, 2721−2730

β-state casts together both the presence of hairpin-like double strand and β turn-like conformation, similarly to ref 61. Despite the high flexibility of switch I, the β secondary structure is poorly sampled in the simulation of the holo ecG$^{\alpha}$·GDP state. Similarly, the α-helical state in the P53−G59 portion of switch I is weakly populated in the ecG$^{\beta}$·GTP simulation; see Figure 3a.

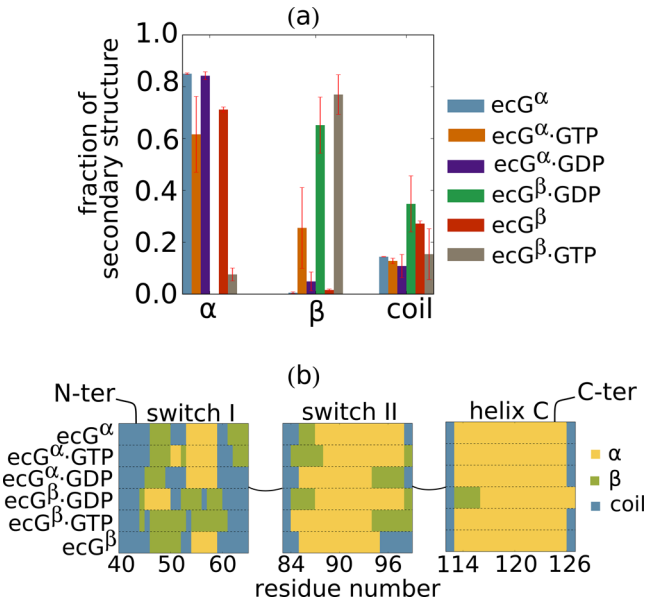

Figure 3. Percentage of secondary structure motifs for a part of the switch I region, residues P53−G59, that is reported to undergo a secondary structure change in the catalytic cycle. The bottom part of the figure shows the most occupied secondary structure per residue for three key regions in the protein, shown for different representative states of the protein during the catalytic cycle.

However, it is interesting to note that the switch I fragment acquires α-helix when ecG$^{\beta}$ is simulated in the apo state. This fact suggests that β to α conformational change during the enzymatic turnover may occur via the ligand-free state. The average secondary structure of two other key regions for protein activity is shown in Figure 3b: the switch II and helix C (residues P113−V125). The switch II is characterized by an extended helix (10 residues) and is found to rigidly shift upon GTP hydrolysis; one turn unfolds at the C-ter side, and one refolds at the N-ter side.[38,49,66] This shift is, for instance, observed in the ecG$^{\alpha}$·GDP, but depending on the initial state, we remark that the extension of the helix is fluctuating across the simulations. The helix C represents the anchoring for the P-loop involved in nucleotide binding.[67] The helical structure is preserved in all of the simulations, meaning that any conformational changes associated with substrate locking are caused by a rigid body motion of this region.

The lack of $\alpha \rightarrow \beta$ transition in the brute force MD of the holo ecG$^{\alpha}$·GDP state could depend on several factors: (i) the presence of a high kinetic barrier separating the two states that would confine the sampling in the initial state only, (ii) an intrinsic bias of the force field used, for instance, it is widely reported that CHARMM22/CMAP favors helical states,[68,69] (iii) the lack of interdomain interactions in our model, in fact the crystallographic evidence of the transition was based on the resolution of the structures of the whole EF-Tu protein, (iv) a temperature effect, since the quench into the two separate states could be caused by the low temperature at which X-ray experiments are performed. In the following, we will address some of these issues.

We have performed enhanced sampling Hamiltonian-replica exchange simulations[50,51] designed to "thermally" excite the switch I region of the protein. The simulations were performed on both holo states of the ecG$^{\alpha}$ conformers (for ecG$^{\beta}$, see the Supporting Information), using 12 replicas for each simulation. According to a mean-field rescaling scheme,[51] the sampling allowed to scan the effective temperature (T_{eff}) window 280−580 K. In Figure 4, we report the fraction of secondary

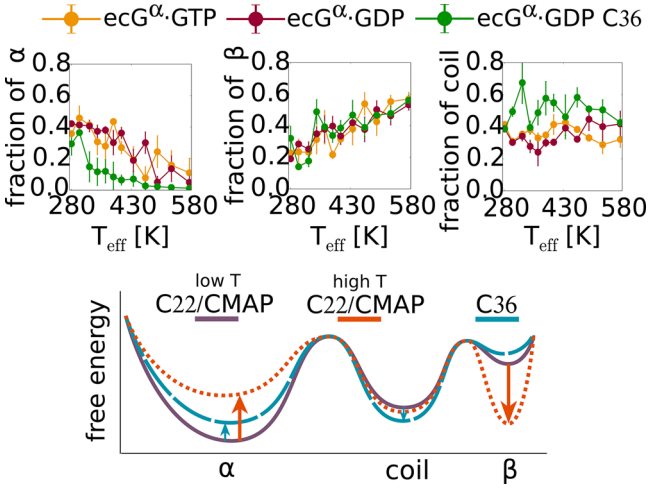

Figure 4. Enhanced sampling of the switch I region in the REST2 simulations. In the top panel, we report the fraction of secondary structures (α, β, coil) in the fragment as a function of the effective temperature exciting the switch I. The lower panel schematically compares data obtained from the simulations of the holo state ecG$^{\alpha}$·GTP(GDP) at different temperatures, based on the CHARMM22/CMAP and CHARMM36 force fields.

structure accessed by the switch I as a function of the effective temperature T_{eff}. We observe that, for both the GTP and GDP ligands, the α conformation is the most populated at ambient conditions, and its occupation decays with temperature. The most important result is the meaningful fraction (20%) of the β-like state—mainly turn—that can be accessed in both of the holo states, and starting from both conformers (see Figure S1 in the Supporting Information). This finding indicates that the α to β transition can occur in our model, although the details of the associated kinetics would require ad-hoc calculations and will be reserved for further work. The population of the β-like structure increases as a function of temperature and compensates the thermal instability of the helical structure. The high, and almost temperature independent, fraction of the unstructured coil state (~40%) further confirms the intrinsic flexibility of the fragment.

In order to account for the force-field dependence of the secondary structure propensities and their relative temperature changes, we have performed simulations of the ecG$^{\alpha}$·GDP state using the CHARMM36 force field, which was designed to give a better helix−coil balance.[70] While the helix state is much less populated, the population of β-like conformation is unchanged when compared to CHARMM22/CMAP. Overall, CHARMM36 renders the fragment highly unstructured, with the coil population being as high as ~50%.

A better sampling of the Hamiltonian-replica exchange could be achieved by extending the simulation time per replica;

DOI: 10.1021/acs.jpcb.6b00306
J. Phys. Chem. B 2016, 120, 2721−2730

however, despite the force field effects, the obtained results clearly show that the α to β conversion in the switch I region is possible. The temperature effect on this transition cannot be rigorously estimated because of present force field inaccuracies.

The Holo States of the Hyperthermophilic G-Domain. In a previous work,[16,52,71] it was observed that the hyperthermophilic apo state ssG spans a comparable and even larger conformational space than the mesophilic variant ecG, and shows well-defined substates separated by high kinetic barriers. The enhanced flexibility is due to the rigid body motion of the highly structured switch I region. Similarly to the case of the homologous mesophilic ecG, the binding of the reactant GTP molecule to the hyperthermophilic domain quenches the protein flexibility. The number of conformational states explored on the same time scale reduces by a factor of 2 with respect to the apo state (Figure 5 and Table S1 in the Supporting Information). In the product holo state ssG·GDP, the protein gets slightly more excited, and it partially recovers its intrinsic flexibility that allows sampling a larger number of kinetically relevant states. This conformational flexibility caused by the GTP hydrolysis localizes at the level of the switch I and II regions (see the bottom part of Figure 5) and is much less pronounced at ambient temperature than in the mesophilic variant. The secondary structure patterns of these regions are quite insensitive to the ligand hydrolysis (see Figure S2 in the Supporting Information), although the switch I of the GTP bound state cages the ligand more extensively by linking the triphospate tail.

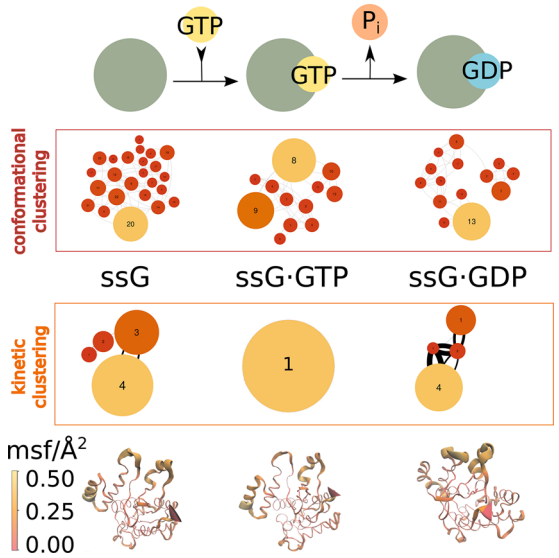

Figure 5. Binding the GTP or GDP to the EF-1α changes the number of representative conformational substates, as shown by both conformational and kinetic clusterings. The lowest panel shows the amplitude of the mean squared fluctuations of the protein backbone, coded in thickness of the backbone representation and color. Data refer to the MD simulations that were performed at T = 300 K.

The increase of conformational entropy in the protein matrix upon catalysis is a signature of functional efficiency, since it relates to both substrate unbinding and long-range communication. Therefore, the weak excitation observed at ambient temperature following the virtual GTP hydrolysis could correlate to the known low activity of the hyperthermophilic domain at ambient conditions. Actually, we see that at high temperature (T= 380 K), slightly exceeding the optimal growth temperature of the *S. solfataricus* archeon, the flexibility of the ssG·GDP is enhanced when compared to ssG·GTP, an increase by a factor of 5, similar to what was found for the mesophilic domain when comparing the reactant ecG$^{\alpha}$·GTP and the product ecG$^{\beta}$·GDP states at ambient conditions; see Table S1 in the Supporting Information. The high temperature release of excitation in ssG·GDP concentrates again mainly in switch I and switch II regions.

WHAT SPECIALIZES THE THERMOPHILIC G-DOMAIN

In the final section, we present a comparative discussion of the molecular factors that cooperate during the enzyme activity of the G-domain in particular, and of the EF protein in general. The focus is first placed on the behavior of the switch I region considered an essential element of the protein matrix to regulate both the ligand binding kinetics and long-range communication upon catalysis.[72] This region has also been pointed out as the weak spot of the mesophilic ecG domain, where the early steps of thermal unfolding take place.[16] In the hyperthermophilic variant ssG, the same region is structurally stabilized by the insertion of two extra small α-helices, α' and α''. By performing enhanced sampling on the two homologues in their holo states via REST2, the stability of the region upon thermal stress has been assessed. In Figure 6, we compare the stability curve obtained for three secondary structure states populated by the fragment in the reactive states of the mesophilic and hyperthermophilic domains, the ecG$^{\alpha}$·GTP and ss·GTP. The mesophilic fragment is not only systematically more flexible at all temperatures, as seen from the higher content of coil, but more importantly, its helical component is shown to be significantly less stable than that of its hyperthermophilic counterpart. The switch I region loses half of its initial fraction of helical content at about T_{eff} = 400 K in the mesophilic ecG$^{\alpha}$·GTP, while for the hyperthermophilic domain, the helical disruption occurs at a much higher value of the effective temperature exciting the fragment. These data confirm that the stability and function of the ssG domain are granted by the more robust structure of its switch I region.

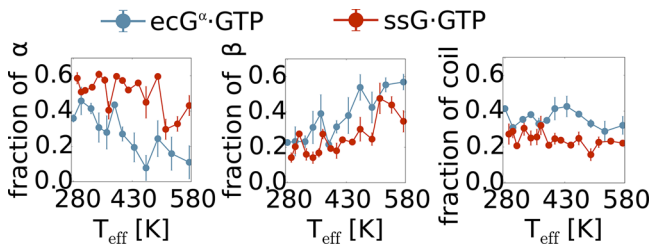

Figure 6. Fraction of secondary structure in the switch I region as a function of temperature for the holo state of the mesophilic and hyperthermophilic domains when bound to the reactive substrate GTP, ecG$^{\alpha}$·GTP, and ssG·GTP, respectively.

A second motif, structurally conserved across EF G-domains, and more broadly in NTPases,[73] acting as a molecular gate for substrate binding and unbinding is the P-loop.[67] The changes in flexibility caused by the substrates is obtained by clustering the conformations explored by this short fragment in the apo and holo states. As it was observed for the global behavior of both proteins, the number of states visited by the P-loop is strongly reduced when the GTP is bound; see Figure 7. The rigidification of the P-loop is the consequence of an extended

DOI: 10.1021/acs.jpcb.6b00306
J. Phys. Chem. B 2016, 120, 2721−2730

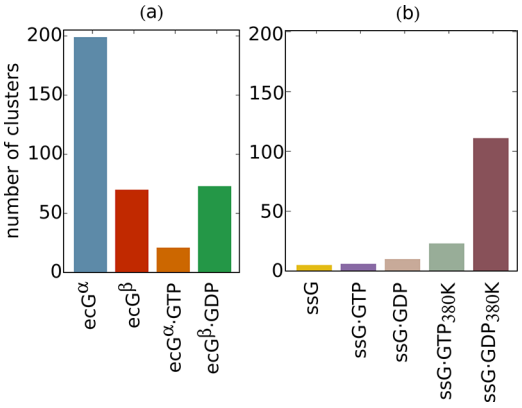

Figure 7. Number of conformational states of the P-loop obtained by cluster analysis of the fragment. Panel a refers to the mesophilic domain, and panel b, to the hyperthermophilic domain. RMSD is used as the collective variable in the clustering, with a cutoff of 0.5 Å.

network of interactions formed with the GTP substrate. This connectivity is graphically represented in the Supporting Information, Figure S3, for both ecG and ssG.

In the mesophilic variant, the rigidification of the P-loop is alleviated when the substrate is changed to GDP and when the product β conformer is considered. This mimics the effect of GTP hydrolysis. The recovered flexibility of the loop is the result of a cooperative effect involving the cleavage of the final phosphate bond of the triposphate tail and the associated conformational change of the switch I region, $\alpha \rightarrow \beta$.[67] The excitation of the loop flexibility upon GTP toward GDP conversion is also found in the hyperthermophilic variant ssG, although no secondary structure change occurs at the level of the switch I. For ssG, the flexibility gap of the switch I between the GTP and GDP bound states further increases when considering the simulations at high temperature (T = 380 K). It is important to stress that only at high temperature the P-loop in ssG·GTP(GDP) exhibits a flexibility comparable to that of the mesophilic domain at ambient conditions. This is an indication of the validity of the corresponding state principle for the involved degrees of freedom. However, a precise connection of the observed variabilities of the P-loop flexibility with the dissociation kinetics of the product molecule GDP is beyond the scope of the present work, since it requires a specialized approach. For example, it is worth mentioning that, when considering the dissociation kinetics of the mant-GTP molecule from EF-Tu, it was surprisingly found that a mutation supposed to increase the local flexibility of the P-loop actually slows down the dissociation kinetics as compared to the wild-type protein.[67] This slowing down is the result of a delicate entropy/enthalpy compensation. The in silico estimate of the enthalpic and entropic contributions to the free energy barrier controlling the substrate dissociation kinetics is challenging because of the difficulties to individuate correct reaction coordinates for the process of interest, and to perform correct sampling.

We conclude by inspecting the correlation between the orientation of His84, a universally conserved residue in translation GTPases,[35,36,74] and the dynamics of the so-called hydrophobic gate (Val20 and Ile61).[34,36] The residue His84 is considered as being a key residue for GTP hydrolysis, and several point mutations of this residue in EF-Tu from *E. coli* showed anticatalytic effects.[35,74] It is however not clear if the role for catalysis is direct, i.e. by activating a water molecule for a nucleophilic attack on the γ-phosphate,[66] or indirect, i.e., by helping the conformational rearrangement of the catalytic site upon ribosome binding.[35] In a cryo-electron microscopic map of the aa-tRNA·EF-Tu·GDP·kirromycin bound to ribosome, and reconstructed by the help of atomistic modeling,[34] the position of the His84 toward the GTP substrate was correlated to the opening of the hydrophobic gate; see PDB 4V69. Although in our simulations we lack the effect of ribosome binding, we explored the dynamics of the hydrophobic gate and of the orientation of His84. The former was monitored by the distance between the side-chain center of mass of the two residues, and the latter, by measuring the distance between the His84 side-chain center of mass and the P_{β} of GTP and GDP molecules. The analysis is extended to the hyperthermophilic domain where, upon structural superimposition, we identified analogous residues.[40,75]

In parts a and b of Figure 8, we report the two-dimensional probability distributions of both distances in GTP and GDP bound states for the two homologous domains ecG and ssG, respectively. For each protein and each holo state, in the top panels, we report the data from MD trajectories and in the bottom panels that from replica exchange simulations. In the mesophilic domain, we find that, although the hydrophobic gate is always in the open state, the His84 is oriented quite far from the GTP molecule. In the cryo-electron microscopy derived structure (PDB code 4V69), the gate distance is about 12 Å, and His84 approaches to P_{β}, 5 Å; see the symbol in Figure 8. Our results show that, in the isolated mesophilic G-domain, the orientation of His84 and the hydrophobic gate are uncorrelated. Interestingly, when moving to the hyperthermophilic ssG, we find that at ambient temperature the analogue of the mesophilic His84, His94 (see sequence alignment in ref 40), is localized far from the catalytic site, at a distance preventing any direct contribution to the GTP hydrolysis. Only at high temperature does the distance decrease to values of ∼6 Å, supporting a possible contribution to the catalysis. The putative analogue of the mesophilic hydrophobic gate in ssG[75] is always found in the open state in our simulations, shown with a dashed line in the figure.

■ CONCLUSIONS

In this work, we have investigated the effect of substrate binding on the conformational flexibility of two homologous GTPase domains of different stability content. In both homologues, the flexibility of the apo protein is readily quenched when the reactant GTP molecule binds to the protein but conversely recovered when the virtual hydrolysis is mimicked by considering the GDP bound state. The flexibility changes are localized at the level of structural key motifs, the switch I, switch II, and the P-loop. The magnitude of the entropy released in the protein matrix upon the reaction differs between the mesophilic and hyperthermophilic enzymes. For the latter, a flexibility of switch I and of P-loop comparable to the mesophilic variant is only attained at high temperature. This finding confirms the validity of the corresponding state principle for these modes, despite the fact that the apo hyperthermophilic domain shows comparable, if not enhanced, flexibility with respect to the apo mesophilic domain. As a final remark, we point out that the stability/function trade-off in the two species relates to the different structure of the switch I region. In the mesophilic domain, the high flexibility of the fragment allows for a secondary structure rearrangement along the functional process but at the same time renders the

DOI: 10.1021/acs.jpcb.6b00306
J. Phys. Chem. B 2016, 120, 2721−2730

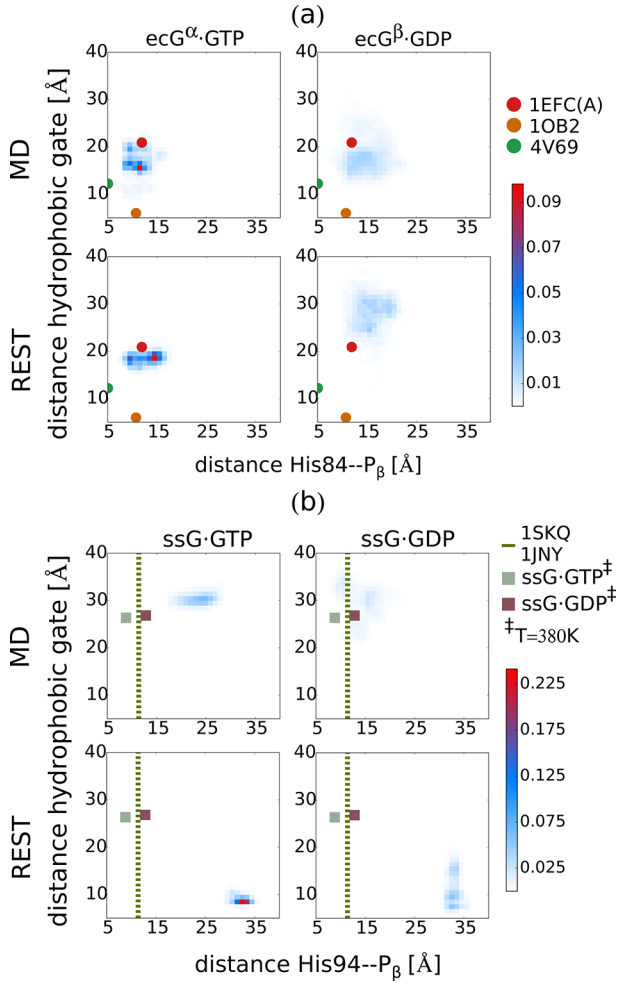

Figure 8. 2D probability distribution of the hydrophobic gate and His84(94)−P$_{\beta}$ distances. The top chart refers to the mesophilic domain, while the bottom chart to the hyperthermophilic domain. For each domain, data are reported for the GTP bound state (left panels) and for the GDP bound state (right panels). For each system, we compare results from MD (top panels of a and b) and REST2 (bottom panels of a and b). Symbols refer to the distances measured in the crystallographic structures indicated in the legend by their PDB codes. For the hyperthermophilic domain, the average value of the hydrophobic gate distance extracted from the simulation at T = 380 K is also reported. The dashed line represents the average His94−P$_{\beta}$ distances in both 1SKQ and 1JNY crystal structures (same value).

fragment highly unstable in temperature. On the other hand, in the hyperthermophilic species, the insertion of extra secondary structure motifs renders the fragment more resistant to temperature, reflecting once again the evolutionary pluralism in optimizing the function in different temperature regimes.

■ ASSOCIATED CONTENT

Supporting Information

The Supporting Information is available free of charge on the ACS Publications website at DOI: 10.1021/acs.jpcb.6b00306.

The details of conformational and kinetic clustering, results of enhanced sampling of the β conformer of the mesophilic domain, details of the secondary structure of the thermophilic species, hydrogen bond patterns, and backbone entropy calculations (PDF)

■ AUTHOR INFORMATION

Corresponding Author

*E-mail: fabio.sterpone@ibpc.fr.

Notes

The authors declare no competing financial interest.

■ ACKNOWLEDGMENTS

The research leading to these results has received funding from the European Research Council under the European Community's Seventh Framework Programme (FP7/2007-2013) Grant Agreement No. 258748. Part of this work was performed using HPC resources from GENCI [CINES and TGCC] (Grant x201576818). We acknowledge the financial support for infrastructures from ANR-11-LABX-0011-01.

■ REFERENCES

(1) Vieille, C.; Zeikus, G. J. Hyperthermophilic enzymes: Sources, Uses, and Molecular Mechanisms for Thermostability. *Microbiol. Mol. Biol. Rev.* **2001**, *65*, 1−43.

(2) Feller, G. Protein Stability and Enzyme Activity at Extreme Biological Temperatures. *J. Phys.: Condens. Matter* **2010**, *22*, 323101.

(3) Somero, G. N. Temperature Adaptation of Enzymes. *Annu. Rev. Ecol. Syst.* **1978**, *9*, 1−29.

(4) Somero, G. N. Proteins and Temperature. *Annu. Rev. Physiol.* **1995**, *57*, 43−68.

(5) Jaenicke, R.; Böhm, G. The Stability of Proteins in Extreme Environments. *Curr. Opin. Struct. Biol.* **1998**, *8*, 738−748.

(6) Kumar, S.; Nussinov, R. How do Thermophilic Proteins Deal with Heat? *Cell. Mol. Life Sci.* **2001**, *58*, 1216−1233.

(7) Sterpone, F.; Melchionna, S. Thermophilic Proteins: Insight and Perspective from In Silico Experiments. *Chem. Soc. Rev.* **2012**, *41*, 1665−1676.

(8) Rathi, P. C.; Höffken, H. W.; Gohlke, H. Quality Matters: Extension of Clusters of Residues with Good Hydrophobic Contacts Stabilize (Hyper)Thermophilic Proteins. *J. Chem. Inf. Model.* **2014**, *54*, 355−361.

(9) Collins, T.; Meuwis, M.-A.; Gerday, C.; Feller, G. Activity, Stability and Flexibility in Glycosidases Adapted to Extreme Thermal Environments. *J. Mol. Biol.* **2003**, *328*, 419−428.

(10) Závodszky, P.; Kardos, J.; Svingor, A.; Petsko, G. A. Adjustment of Conformational Flexibility is a Key Event in the Thermal Adaptation of Proteins. *Proc. Natl. Acad. Sci. U. S. A.* **1998**, *95*, 7406−7411.

(11) Hernandez, G.; Jenney, F. E.; Adams, M. W. W.; LeMaster, D. M. Millisecond Time Scale Conformational Flexibility in a Hyperthermophile Protein at Ambient Temperature. *Proc. Natl. Acad. Sci. U. S. A.* **2000**, *97*, 3166−3170.

(12) Kohen, A.; Klinman, J. P. Protein Flexibility Correlates with Degree of Hydrogen Tunneling in Thermophilic and Mesophilic Alcohol Dehydrogenases. *J. Am. Chem. Soc.* **2000**, *122*, 10738−10739.

(13) Lazaridis, T.; Lee, I.; Karplus, M. Dynamics and Unfolding Pathways of a Hyperthermophilic and a Mesophilic Rubredoxin. *Protein Sci.* **1997**, *6*, 2589−2605.

(14) Roca, M.; Liu, H.; Messer, B.; Warshel, A. On the Relationship Between Thermal Stability and Catalytic Power of Enzymes. *Biochemistry* **2007**, *46*, 15076−88.

(15) Merkley, E. D.; Parson, W. W.; Daggett, V. Temperature Dependence of the Flexibility of Thermophilic and Mesophilic Flavoenzymes of the Nitroreductase Fold. *Protein Eng., Des. Sel.* **2010**, *23*, 327−36.

(16) Kalimeri, M.; Rahaman, O.; Melchionna, S.; Sterpone, F. How Conformational Flexibility Stabilizes the Hyperthermophilic Elongation Factor G-Domain. *J. Phys. Chem. B* **2013**, *117*, 13775−13785.

(17) Radestock, S.; Gohlke, H. Protein Rigidity and Thermophilic Adaptation. *Proteins: Struct., Funct., Genet.* **2011**, *79*, 1089−1108.

DOI: 10.1021/acs.jpcb.6b00306
J. Phys. Chem. B 2016, 120, 2721−2730

(18) Rathi, P. C.; Jaeger, K.-E.; Gohlke, H. Structural Rigidity and Protein Thermostability in Variants of Lipase A from Bacillus Subtilis. *Plos One* **2015**, *10*, e0130289.
(19) Kohen, A.; Klinman, J. P. Protein Flexibility Correlates with Degree of Hydrogen Tunneling in Thermophilic and Mesophilic Alcohol Dehydrogenases. *J. Am. Chem. Soc.* **2000**, *122*, 10738−10739.
(20) Kohen, A.; Cannio, R.; Bartolucci, S.; Klinman, J. P. Enzyme Dynamics and Hydrogen Tunnelling in a Thermophilic Alcohol Dehydrogenase. *Nature* **1999**, *399*, 496−499.
(21) Olsson, M. H. M.; Parson, W. W.; Warshel, A. Dynamical Contributions to Enzyme Catalysis: Critical Tests of A Popular Hypothesis. *Chem. Rev.* **2006**, *106*, 1737−1756.
(22) Kim, H. S.; Damo, S. M.; Lee, S.-Y.; Wemmer, D.; Klinman, J. P. Structure and Hydride Transfer Mechanism of a Moderate Thermophilic Dihydrofolate Reductase from Bacillus Stearothermophilus and Comparison to Its Mesophilic and Hyperthermophilic Homologues. *Biochemistry* **2005**, *44*, 11428−11439.
(23) Guo, J.; Loveridge, E. J.; Luk, L. Y. P.; Allemann, R. K. Effect of Dimerization on Dihydrofolate Reductase Catalysis. *Biochemistry* **2013**, *52*, 3881−3887.
(24) Luk, L. Y. P.; Loveridge, E. J.; Allemann, R. K. Different Dynamical Effects in Mesophilic and Hyperthermophilic Dihydrofolate Reductases. *J. Am. Chem. Soc.* **2014**, *136*, 6862−6865.
(25) Chakraborty, D.; Taly, A.; Sterpone, F. Stay Wet, Stay Stable? How Internal Water Helps the Stability of Thermophilic Proteins. *J. Phys. Chem. B* **2015**, *119*, 12760−12770.
(26) Kalimeri, M.; Girard, E.; Madern, D.; Sterpone, F. Interface Matters: The Stiffness Route to Stability of a Thermophilic Tetrameric Malate Dehydrogenase. *PLoS One* **2014**, *9*, e113895.
(27) Wolf-Watz, M.; Thai, V.; Henzler-Wildman, K.; Hadjipavlou, G.; Eisenmesser, E.; Kern, D. Linkage Between Dynamics and Catalysis in a Thermophilic-mesophilic Enzyme Pair. *Nat. Struct. Mol. Biol.* **2004**, *11*, 945−949.
(28) Tehei, M.; Madern, D.; Franzetti, B.; Zaccai, G. Neutron Scattering Reveals the Dynamic Basis of Protein Adaptation to Extreme Temperature. *J. Biol. Chem.* **2005**, *280*, 40974−40979.
(29) Marcos, E.; Mestres, P.; Crehuet, R. Crowding Induces Differences in the Diffusion of Thermophilic and Mesophilic Proteins: A New Look at Neutron Scattering Results. *Biophys. J.* **2011**, *101*, 2782−2789.
(30) Calligari, P. A.; Calandrini, V.; Ollivier, J.; Artero, J.-B.; Härtlein, M.; Johnson, M.; Kneller, G. R. Adaptation of Extremophilic Proteins with Temperature and Pressure: Evidence from Initiation Factor 6. *J. Phys. Chem. B* **2015**, *119*, 7860−7873.
(31) Kavaliauskas, D.; Nissen, P.; Knudsen, C. R. The Busiest of All Ribosomal Assistants: Elongation Factor Tu. *Biochemistry* **2012**, *51*, 2642−2651.
(32) Andersen, G. R.; Nissen, P.; Nyborg, J. Elongation Factors in Protein Biosynthesis. *Trends Biochem. Sci.* **2003**, *28*, 434−441.
(33) Pape, T.; Wintermeyer, W.; Rodnina, M. V. Complete Kinetic Mechanism of Elongation Factor Tu-dependent Binding of Aminoacyl-tRNA to the A Site of the E. Coli Ribosome. *EMBO J.* **1998**, *17*, 7490−7497.
(34) Villa, E.; Sengupta, J.; Trabuco, L. G.; LeBarron, J.; Baxter, W. T.; Shaikh, T. R.; Grassucci, R. A.; Nissen, P.; Ehrenberg, M.; Schulten, K.; et al. Ribosome-induced Changes in Elongation Factor Tu Conformation Control GTP Hydrolysis. *Proc. Natl. Acad. Sci. U. S. A.* **2009**, *106*, 1063−1068.
(35) Adamczyk, A. J.; Warshel, A. Converting Structural Information into an Allosteric-energy-based Picture for Elongation Factor Tu Activation by the Ribosome. *Proc. Natl. Acad. Sci. U. S. A.* **2011**, *108*, 9827−9832.
(36) Voorhees, R. M.; Schmeing, T. M.; Kelley, A. C.; Ramakrishnan, V. The Mechanism for Activation of GTP Hydrolysis on the Ribosome. *Science* **2010**, *330*, 835−838.
(37) Fischer, N.; Neumann, P.; Konevega, A. L.; Bock, L. V.; Ficner, R.; Rodnina, M. V.; Holger, S. Structure of the E. Coli Ribosome-EF-Tu Complex at < 3 A Resolution by Cs-corrected Cryo-EM. *Nature* **2015**, *520*, 567−570.
(38) Song, H.; Parsons, M. R.; Rowsell, S.; Leonard, G.; Phillips, S. E. Crystal Structure of Intact Elongation Factor EF-Tu from Escherichia Coli in GDP Conformation at 2.05 Å Resolution. *J. Mol. Biol.* **1999**, *285*, 1245−1256.
(39) Šanderová, H.; Hůlková, M.; Maloň, P.; Kepková, M.; Jonák, J. Thermostability of Multidomain Proteins: Elongation Factors EF-Tu from Escherichia Coli and Bacillus Stearothermophilus and their Chimeric Forms. *Protein Sci.* **2004**, *13*, 89−99.
(40) Vitagliano, L.; Ruggiero, A.; Masullo, M.; Cantiello, P.; Arcari, P.; Zagari, A. The Crystal Structure of Sulfolobus Solfataricus Elongation Factor 1a in Complex with Magnesium and GDP. *Biochemistry* **2004**, *43*, 6630−6636.
(41) Vitagliano, L.; Masullo, M.; Sica, F.; Zagari, A.; Bocchini, V. The Crystal Structure of Sulfolobus Solfataricus Elongation Factor 1 in Complex with GDP Reveals Novel Features in Nucleotide Binding and Exchange. *EMBO J.* **2001**, *20*, 5305−5311.
(42) Parmeggiani, A.; Swart, G.; Mortensen, K. K.; Jensen, M.; Clark, B. F.; Dente, L.; Cortese, R. Properties of a Genetically Engineered G Domain of Elongation Factor Tu. *Proc. Natl. Acad. Sci. U. S. A.* **1987**, *84*, 3141−3145.
(43) Masullo, M.; Ianniciello, G.; Arcari, P.; Bocchini, V. Properties of Truncated Forms of the Elongation Factor 1 from the Archaeon Sulfolobus Solfataricus. *Eur. J. Biochem.* **1997**, *243*, 468−473.
(44) Jensen, M.; Cool, R.; Mortensen, K.; Clark, B.; Parmeggiani, A. Structure-function Relationships of Elongation Factor Tu. Isolation and Activity of the Guanine-nucleotide-binding Gomain. *Eur. J. Biochem.* **1989**, *182*, 247−255.
(45) Šanderová, H.; TiŠerová, H.; Barvík, I.; Sojka, L.; Jonák, J.; Krásný, L. The N-terminal Region is Crucial for the Thermostability of the G-domain of Bacillus. *Biochim. Biophys. Acta, Proteins Proteomics* **2010**, *1804*, 147−155.
(46) Stouten, P. F.; Sander, C.; Wittinghofer, A.; Valencia, A. How Does The Switch II Region of G-Domains Work? *Febs Lett.* **1993**, *320*, 1−6.
(47) Thomas, C. J.; Du, X.; Li, P.; Wang, Y.; Ross, E. M.; Sprang, S. R. Uncoupling Conformational Change from GTP Hydrolysis in a Heterotrimeric G Protein Alpha-Subunit. *Proc. Natl. Acad. Sci. U. S. A.* **2004**, *101*, 7560−7565.
(48) Abel, K.; Yoder, M. D.; Hilgenfeld, R.; Jurnak, F. An α to β Conformational Switch in EF-Tu. *Structure* **1996**, *4*, 1153−1159.
(49) Polekhina, G.; Thirup, S.; Kjeldgaard, M.; Nissen, P.; Lippmann, C.; Nyborg, J. Helix Unwinding in the Effector Region of Elongation Factor EF-Tu-GDP. *Structure* **1996**, *4*, 1141−1151.
(50) Wang, L.; Friesner, R.; Berne, B. Replica Exchange with Solute Scaling: a more Efficient Version of Replica Exchange with Solute Tempering (REST2). *J. Phys. Chem. B* **2011**, *115*, 9431−9438.
(51) Stirnemann, G.; Sterpone, F. Recovering Protein Thermal Stability Using All-Atom Hamiltonian Replica-Exchange Simulations in Explicit Solvent. *J. Chem. Theory Comput.* **2015**, *11*, 5573−5577.
(52) Sterpone, F.; Bertonati, C.; Briganti, G.; Melchionna, S. Key Role of Proximal Water in Regulating Thermostable Proteins. *J. Phys. Chem. B* **2009**, *113*, 131−137.
(53) Phillips, J. C.; Braun, R.; Wang, W.; Gumbart, J.; Tajkhorshid, E.; Villa, E.; Chipot, C.; Skeel, R. D.; Kalé, L.; Schulten, K. Scalable Molecular Dynamics with NAMD. *J. Comput. Chem.* **2005**, *26*, 1781−1802.
(54) MacKerell, A. D.; Bashford, D.; Bellott, M.; Dunbrack, R. L.; Evanseck, J. D.; Field, M. J.; Fischer, S.; Gao, J.; Guo, H.; Ha, S.; et al. All-Atom Empirical Potential for Molecular Modeling and Dynamics Studies of Proteins. *J. Phys. Chem. B* **1998**, *102*, 3586−3616.
(55) MacKerell, A. D.; Feig, M.; Brooks, C. L., III Extending the Treatment of Backbone Energetics in Protein Force Fields: Limitations of Gas-phase Quantum Mechanics in Reproducing Protein Conformational Distributions in Molecular Dynamics Simulations. *J. Comput. Chem.* **2004**, *25*, 1400−1415.
(56) Darden, T.; York, D.; Pedersen, L. Particle Mesh Ewald: An NÂlog(N) Method for Ewald Sums in Large Systems. *J. Chem. Phys.* **1993**, *98*, 10089−10092.

DOI: 10.1021/acs.jpcb.6b00306
J. Phys. Chem. B 2016, 120, 2721−2730

(57) Best, R. B.; Zhu, X.; Shim, J.; Lopes, P. E. M.; Mittal, J.; Feig, M.; Alexander, D.; MacKerell, J. Optimization of the Additive CHARMM All-Atom Protein Force Field Targeting Improved Sampling of the Backbone, and Side-Chain 1 and 2 Dihedral Angles. *J. Chem. Theory Comput.* **2012**, *8*, 3257−3273.
(58) Hartigan, J. *Clustering Algorithms*; Wiley: New York, 1975.
(59) Bastian, M.; Heymann, S.; Jacomy, M. Gephi: An Open Source Software for Exploring and Manipulating Networks. International AAAI Conference on Weblogs and Social Media, 2009.
(60) van Dongen, S. M. Graph Clustering by Flow Simulation. Ph.D. Thesis, University of Utrecht, The Netherlands, 2000.
(61) Kulczycka, K.; Długosz, M.; Trylska, J. Molecular Dynamics of Ribosomal Elongation Factors G and Tu. *Eur. Biophys. J.* **2011**, *40*, 289−303.
(62) Yang, D.; Kay, L. Contributions to Conformational Entropy Arising from Bond Vector Fluctuations Measured from NMR-derived Order Parameters: Application to Protein Folding. *J. Mol. Biol.* **1996**, *263*, 369−382.
(63) Bui, J. M.; Gsponer, J.; Vendruscolo, M.; Dobson, C. M. Analysis of Sub-c and Supra-c Motions in Protein G1 Using Molecular Dynamics Simulations. *Biophys. J.* **2009**, *97*, 2513−2520.
(64) English, B. P.; Min, W.; van Oijen, A.; Lee, K.; Luo, G.; Sun, H.; Cherayil, B.; Kou, S.; Xie, X. Ever-fluctuating Single Enzyme Molecules: Michaelis-Menten Equation Revisited. *Nat. Chem. Biol.* **2006**, *2*, 87−94.
(65) Vogeley, L.; Palm, G. J.; Mesters, J. R.; Hilgenfeld, R. Conformational Change of Elongation Factor Tu (EF-Tu) Induced by Antibiotic Binding. *J. Biol. Chem.* **2001**, *276*, 17149−17155.
(66) Kjeldgaard, M.; Nissen, P.; Thirup, S.; Nyborg, J. The Crystal Structure of Elongation Factor EF-Tu from Thermus Aquaticus in the GTP Conformation. *Structure* **1993**, *1*, 35−50.
(67) Mercier, E.; Girodat, D.; Wieden, H.-J. A Conserved P-loop Anchor Limits the Structural Dynamics that Mediate Nucleotide Dissociation in EF-Tu. *Sci. Rep.* **2015**, *5*, 7677.
(68) Lindorff-Larsen, K.; Maragakis, P.; Piana, S.; Eastwood, M. P.; Dror, R. O.; Shaw, D. E. Systematic Validation of Protein Force Fields against Experimental Data. *PLoS One* **2012**, *7*, e32131.
(69) Cino, E. A.; Choy, W.-Y.; Karttunen, M. Comparison of Secondary Structure Formation Using 10 Different Force Fields in Microsecond Molecular Dynamics Simulations. *J. Chem. Theory Comput.* **2012**, *8*, 2725−2740.
(70) Huang, J.; MacKerell, A. D. CHARMM36 All-atom Additive Protein Force Field: Validation Based on Comparison to NMR Data. *J. Comput. Chem.* **2013**, *34*, 2135−2145.
(71) Rahaman, O.; Kalimeri, M.; Melchionna, S.; Hénin, J.; Sterpone, F. Role of Internal Water on Protein Thermal Stability: The Case of Homologous G Domains. *J. Phys. Chem. B* **2015**, *119*, 8939−8949.
(72) Abel, K.; Jurnak, F. A Complex Profile of Protein Elongation: Translating Chemical Energy into Molecular Movement. *Structure* **1996**, *4*, 229−238.
(73) Wittinghofer, A.; Vetter, I. R. Structure-Function Relationships of the G Domain, a Canonical Switch Motif. *Annu. Rev. Biochem.* **2011**, *80*, 943−971.
(74) Cool, R. H.; Parmeggiani, A. Substitution of Histidine-84 and the GTPase Mechanism of Elongation Factor Tu. *Biochemistry* **1991**, *30*, 362−366.
(75) Kobayashi, K.; Kikuno, I.; Kuroha, K.; Saito, K.; Ito, K.; Ishitani, R.; Inada, T.; Nurekia, O. Structural Basis for mRNA Surveillance by Archaeal Pelota and GTP-bound EF1 Complex. *Proc. Natl. Acad. Sci. U. S. A.* **2010**, *107*, 17575−17579.

DOI: 10.1021/acs.jpcb.6b00306
J. Phys. Chem. B 2016, 120, 2721−2730